Modeling Fracture in Carbon Nanotubes Using a Meshless Atomic-Scale Finite-Element Method

Xue Feng, Hanqing Jiang, Yonggang Huang, Bin Liu, and Jiun-Shyan Chen

A meshless atomic-scale computational method was developed by taking account of structural dynamic evolution, such as atomic bond breakage and regeneration. This method, based on energy minimization, is an extension of B. Liu et al.'s atomic-scale finite element method (AFEM). The proposed method is faster than the standard conjugate gradient method and AFEM and can thus significantly save computational time especially in studying large-scale problems. The bond breakage of single-wall carbon nanotubes was studied.

INTRODUCTION

The ultimate goal of nanotechnology is to produce multifunctional materials directly from atoms in what is known as the "bottom-up" method. In order to realize this significant prospect, multiscale simulations encompassing atomic information and macroscopic objects emerged and have become a highly pursued research area.[1] Large-scale, high-efficiency computing is playing an important and active part in the development of multiscale simulations. Nowadays, the fastest supercomputer in the world can handle up to a billion atoms in molecular dynamics simulations,[2,3] which only corresponds to a small cube of 1 μm in size. Even with rapid advances in computer power, this size may increase to 10 μm in 15 years since the computer power doubles every 18 months (Moore's law[4]). Therefore, molecular dynamics simulations alone cannot predict the properties and response of macroscopic materials directly from their nano- and microstructures. Other atomistic methods also have difficulties for large scales. For example, the widely used conjugate gradient method in molecular mechanics as well as in molecular dynamics is an order-N^2 method for which the computational effort is proportional to the square of the system size N (e.g., number of atoms). Therefore, the existing atomistic simulations cannot scale up for multiscale simulations.

On the other hand, conventional continuum methods such as the finite element method (FEM) are not applicable to nanoscale components because they were developed for macroscale problems. The phenomenological material constitutive models make conventional continuum methods unable to capture the nanoscale nature. These continuum constitutive models in conventional FEM cannot accurately predict the responses of discrete atoms since they represent the collective behavior of many atoms. Furthermore, most atomistic interactions are multi-body in nature (i.e., the energy in an atomic bond between a pair of atoms depends on the positions of atoms both in and outside the pair [e.g., References 5 and 6]). This non-local dependence of energy cannot be considered by the macroscopic, local constitutive model in the conventional FEM.

An obvious gap exists between the atomistic simulations and continuum FEM; therefore, multiscale computational methods have emerged as a viable means to study materials and systems across different length scales.[7–23] The idea is to combine the continuum FEM, which represents the collective behavior of atoms but significantly reduces the degrees of freedom, with atomistic simulation methods that accurately capture nanoscale physical laws.

One approach is to use the atomistic simulation methods for domains in which the discrete motion of atoms is important and must be accounted for, and use the continuum FEM for the rest where the response of materials and systems can be represented by the continuum models.[9–13] Artificial interfaces between atomistic and continuum domains were introduced to bridge these two domains, which require interfacial conditions and add significant computational efforts, and therefore may lead to computational errors.

Another approach in the atomistic–continuum linkage is the quasicontinuum method,[24–29] which involves both discrete atoms and continuum solids. This method can also account for nonlocal effects. The continuum solids are characterized based on the interatomic potential (multi-body atomistic interactions) via the Cauchy–Born rule[30]

How would you...

...describe the overall significance of this paper?

An atomic-scale computational method is proposed in this paper which is faster than the standard conjugate gradient. This method is powerful for simulating dynamic structural evolution, such as bond breakage and regeneration of nanotubes.

...describe this work to a materials science and engineering professional with no experience in your technical specialty?

An atomic-scale computational method is proposed that takes advantage of both molecular mechanics and the finite element method. This method runs faster than the conjugate gradient method and can simulate the structural dynamic evolution of a nanotube.

...describe this work to a layperson?

An atomic-scale computational method is proposed that runs faster than conventional methods. Also, this method can simulate the dynamic evolution of nanotubes, such as cracking propagation.

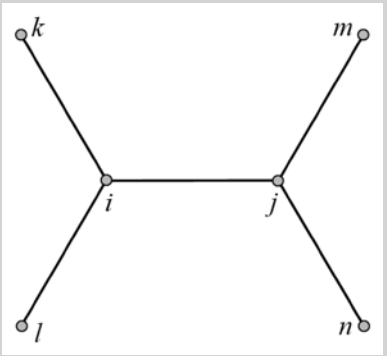

Figure 1. The atomic bond between carbon atoms i and j, as well as their first nearest-neighbor atoms.

in which the continuum strain energy density is obtained from the energy stored in atomic bonds. However, ghost force appears at the interface between the domains of (local) continuum and (non-local) atomistic simulations in the quasicontinuum method.[24] Moreover, the quasicontinuum analysis uses the conjugate gradient method,[27] which is an order-N^2 method and is not suitable for large problems.

Recently, B. Liu et al.[31,32] developed an atomic-scale finite-element method (AFEM) that is faster and as accurate as molecular mechanics simulations. The method deals with discrete atoms that interact according to multi-body atomistic potential. Depending on multi-body atomistic interactions, a material-specific element was developed to include the nonlocal effect within a single element. Compared with the widely used conjugate gradient method, AFEM is a fast method for convergence on static equilibrium positions. Since AFEM has the same theoretical framework of conventional FEM, AFEM and conventional FEM combined provide a powerful tool for static multiscale simulations.

Elements play an important role in the development of AFEM to include the multi-body atomistic interactions in the framework of conventional FEM. However, elements also introduce a drawback for AFEM: atomic structural evolution needs additional efforts to regenerate elements and thus additional computational costs are required. In order to overcome this drawback and keep the advantage of AFEM (i.e., the multi-body atomistic interactions in the framework of FEM), the authors extended AFEM by a meshless method. The existing AFEM has to establish the mesh and element in the computation as the conventional FEM. However, the proposed meshless AFEM involves no "element." The common elements ensemble does not exist anymore and therefore the meshless AFEM is more computationally efficient than AFEM. The atomic structural evolution, such as bonding breaking and fracture, can be coherently studied without involving additional computational costs to re-generate elements.

Since both the meshless AFEM and the original AFEM depend on the nature of multi-body atomistic interactions, the multi-body atomistic interaction for carbon were studied.

MULTI-BODY INTERATOMIC POTENTIAL FOR CARBON

The Brenner potential[6] is expressed as Equation 1, where i and j denote two carbon atoms at the ends of the bond, and r_{ij} is the bond length. V_R and V_A are the pair terms (i.e., depending only on the bond length r_{ij}) that represent the repulsive and attractive interactions of the carbon atoms, and are given by Equations 2 and 3. (All equations are shown in the table.)

The parameters $D^{(e)}$, S, β, and $R^{(e)}$ are determined by fitting with known physical properties of various types of carbon. In particular, $R^{(e)}$ represents the equilibrium distance of two freestanding carbon atoms (i.e., without other atoms involved). The function f_c is merely a smooth cut-off function to limit the range of interaction between carbon atoms, and it is given by Equation 4, where the effective range of the cut-off function is defined by $R^{(1)}$ and $R^{(2)}$. Specifically, $R^{(1)}$ and $R^{(2)}$ are chosen so as to account for interactions among only the nearest-neighbor carbon atoms.

The term B_{ij} in Equation 1 represents a multi-body coupling term, which results from the interaction between atoms i, j, and their local environment, and is given by Equation 5, where k denotes carbon atoms other than i and j, r_{ik} is the distance between carbon atoms i and k, and δ is another fitting parameter. f_c is the aforementioned cut-off function in Equation 4, and θ_{ijk} defines the angle between carbon bonds i–j and i–k, as shown in Figure 1. The function G is given by Equation 6, where a_0, c_0, and d_0 are all fitting parameters given by Brenner.[6] Equation 5 clearly shows that the potential energy for bond i–j depends on other atoms (e.g., k, m), which is the multi-body interactions.

D.W. Brenner[6] determined the parameters $D^{(e)}$, S, β, $R^{(e)}$, $R^{(1)}$, $R^{(2)}$, δ, a_0, c_0, and d_0 as

$D^{(e)} = 6.000$ eV, $S = 1.22$, $\beta = 21$ nm^{-1}

$R^{(e)} = 0.1390$ nm

$R^{(1)} = 0.17$ nm, $R^{(2)} = 0.20$ nm

$\delta = 0.50000$

$a_0 = 0.00020813$, $c_0 = 330$, $d_0 = 3.5$

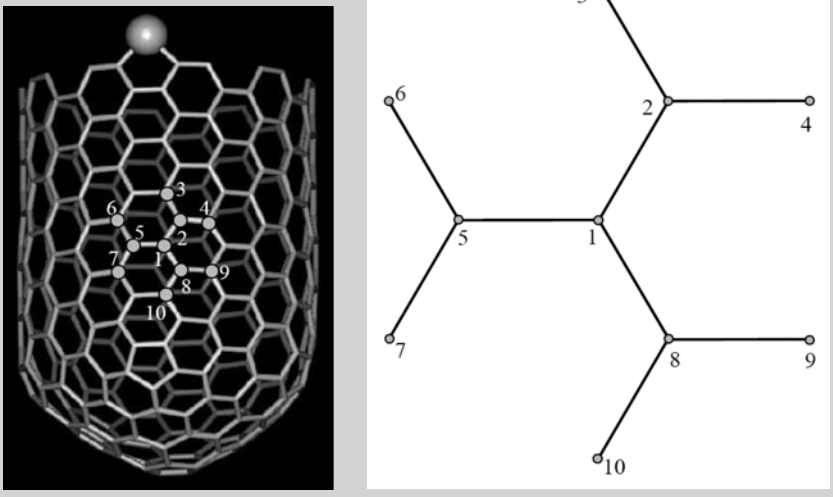

a b

Figure 2. (a) Atom 1 marked as a central atom, along with its neighboring atoms, in a cylindrical carbon nanotube; (b) the AFEM element for central atom 1, which consists of three nearest-neighbor atoms and six second nearest-neighbor atoms.

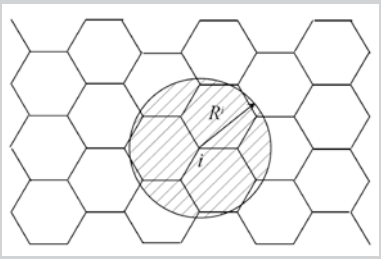

Figure 3. The interaction range of atom "i".

by fitting the lattice constants and binding energies of graphite, diamond, simple cubic, and face-centered-cubic (fcc) carbon, as well as vacancy formation energies of graphite and diamond.

ATOMIC-SCALE FINITE-ELEMENT METHOD: A BRIEF REVIEW

The basic concept on which AFEM is built is static equilibrium, which corresponds to a state of minimal energy. Therefore, AFEM seeks to identify a minimal energy state and has the same theoretical framework of conventional FEM. The difference between AFEM and conventional FEM is the former deals with discrete atoms while the latter focuses on a finite number of elements and nodes.

For a system of N atoms, the total potential energy stored in the atomic bonds is given in Equation 7, where $U_{tot}(\mathbf{x})$ is the atomistic potential energy (e.g., Brenner's potential for carbon) that depends on the atom positions $\mathbf{x} = \mathbf{x}_1, \mathbf{x}_2, \ldots, \mathbf{x}_N)^T$, and $\bar{\mathbf{F}}_i$ is the external force (if there is any) exerted on atom "i." The state of minimal energy corresponds to Equation 8.

The Taylor expansion of E_{tot} around an initial position $\mathbf{x}^{(0)} = (\mathbf{x}_1^{(0)}, \mathbf{x}_2^{(0)}, ..., \mathbf{x}_N^{(0)})^T$ (that is usually not corresponding to equilibrium) gives Equation 9.

The governing equation for the displacement $\mathbf{u} = \mathbf{x} - \mathbf{x}^{(0)}$ is obtained by substituting Equation 9 into Equation 8 as shown in Equation 10. Equation 11 is the stiffness matrix, Equation 12 is the non-equilibrium force vector, and $\bar{\mathbf{F}} = (\bar{\mathbf{F}}_1, \bar{\mathbf{F}}_2, ..., \bar{\mathbf{F}}_N)^T$. The stiffness matrix **K** and non-equilibrium force vector **P** are evaluated in each iteration step. Equation 10 is solved iteratively until $\mathbf{P} = 0$. The governing equation (Equation 10) is the same as that for conventional FEM and that is why AFEM has the same theoretical framework as conventional FEM.

Since both **K** and **P** depend on the interatomic potential energy either from the second-order or first-order derivatives of the potential energy U_{tot}, the AFEM elements are material specific (i.e., they depend on the atomic structure and nearest-neighbor and second nearest-neighbor interactions). An AFEM element for carbon nanotubes is shown in Figure 2. As shown in Figure 2a, each carbon atom (e.g., atom #1) on a carbon nanotube interacts with three nearest-neighbor (local) atoms (e.g., 2, 5, and 8) and six second nearest-neighbor (nonlocal) atoms (e.g., 3, 4, 6, 7, 9, and 10). The AFEM element therefore consists of 10 carbon atoms (Figure 2b), namely the central atom 1, nearest-neighbor atoms 2, 5, and 8, and second nearest-neighbor atoms 3, 4, 6, 7, 9, and 10. Such an element captures the nonlocal interactions between the central atom and other atoms in this single element.

The element stiffness matrix and the non-equilibrium force vector are then given by Equations 13 and 14, where i ranges from 2 to 10 in $\frac{\partial^2 U_{tot}}{\partial \mathbf{x}_1 \partial \mathbf{x}_i}$, and $\bar{\mathbf{F}}_1$ is the external force (if there is any) exerted on the central atom in this element. It is noticeable that the non-zero components in the above element stiffness matrix are limited to the top three rows and the left three columns, which is very different from the element stiffness matrix in conventional FEM be-

Equations

$$V(r_{ij}) = V_R(r_{ij}) - \frac{1}{2}(B_{ij} + B_{ji})\, V_A(r_{ij}) \tag{1}$$

$$V_R(r) = \frac{D^{(e)}}{S-1} e^{-\sqrt{2s}\beta\left(r - R^{(e)}\right)} f_c(r) \tag{2}$$

$$V_A(r) = \frac{D^{(e)} S}{S-1} e^{-\sqrt{\frac{2}{s}}\beta\left(r - R^{(e)}\right)} f_c(r) \tag{3}$$

$$f_c(r) = \begin{cases} 1 & r < R^{(1)} \\ \frac{1}{2}\left\{1 + \cos\left[\frac{\pi\left(r - R^{(1)}\right)}{R^{(2)} - R^{(1)}}\right]\right\} & R^{(1)} < r < R^{(2)} \\ 0 & r > R^{(2)} \end{cases} \tag{4}$$

$$B_{ij} = \left[1 + \sum_{k(\neq i,j)} G(\theta_{ijk}) f_c(r_{ik})\right]^{-\delta} \tag{5}$$

$$G(\theta) = a_0\left[1 + \frac{c_0^2}{d_0^2} - \frac{c_0^2}{d_0^2 + (1 + \cos\theta)^2}\right] \tag{6}$$

$$E_{tot}(\mathbf{x}) = U_{tot}(\mathbf{x}) - \sum_{i=1}^{N} \bar{\mathbf{F}}_i \cdot \mathbf{x}_i \tag{7}$$

$$\frac{\partial E_{tot}}{\partial \mathbf{x}} = 0 \tag{8}$$

$$E_{tot}(\mathbf{x}) \approx E_{tot}(\mathbf{x}^{(0)}) + \left.\frac{\partial E_{tot}}{\partial \mathbf{x}}\right|_{\mathbf{x}=\mathbf{x}^{(0)}} \cdot (\mathbf{x} - \mathbf{x}^{(0)}) + \frac{1}{2}(\mathbf{x} - \mathbf{x}^{(0)})^T \cdot \left.\frac{\partial^2 E_{tot}}{\partial \mathbf{x} \partial \mathbf{x}}\right|_{\mathbf{x}=\mathbf{x}^{(0)}} \cdot (\mathbf{x} - \mathbf{x}^{(0)}) \tag{9}$$

cause the AFEM element focuses on the central atom. In other words, there are "N" AFEM elements for a system with "N" atoms.

Despite the same theoretical framework of FEM and AFEM, AFEM has several distinctions with FEM. First, AFEM takes atoms as FEM notes so there are no shape functions to interpolate with the element. Second, an AFEM element for carbon overlaps in space with neighbor elements.

In fact, this overlap enables one to accurately account for the nonlocal (multi-body) effect within a single element. Such an overlap does not double count the element contribution to the global stiffness matrix **K** and non-equilibrium force vector **P** due to the factor 1/2.

MESHLESS ATOMIC-SCALE FINITE ELEMENT METHOD

The AFEM element, for example the element for carbon shown in Figure 2b, is a key concept to consider the nonlocal atomistic interactions within a single element. However, this element also leads to some restrictions in some applications when the structural evolution occurs. Structural evolution includes bond breaking and formation, which change the conformation of element. For instance, if bond 2–3 breaks in Figure 2b, atom 1 does not interact with atom 3 and therefore the element with atom 1 as the central atom will change. This element conformation change will cause re-meshing, which requires significant computational resources if conducted by existing AFEM.

Interaction Range

Atomistic interactions are short-ranged, which means that one atom only interacts with a limited number of atoms nearby. For carbon nanotubes, as shown in Figure 2b, one atom only interacts with 9 atoms, three nearest-neighbor atoms (local), and six second nearest-neighbor atoms (nonlocal). In fact, the number of atoms involved in a single element is determined by the cutoff distance, such as $R^{(2)} = 0.2$ nm for Brenner's[6] potential. Therefore, instead of the involvement of an AFEM element, the nonlocal effect can be simply characterized by the interaction range (0.2 nm, for instance, for carbon).

For an atom i, the interaction range R^i is given by the interatomic potential. Figure 3, for example, shows the interaction range R^i for carbon atom i, where the atoms inside this range R^i have interactions with atom i, while those outside the circle do not interact with atom i. Therefore, the component of the stiffness matrix **K** can be expressed as Equation 15.

Thus for each atom in the system, the stiffness matrix **K** and non-equilibrium force vector **P** are calculated by the summation of the contributions of all atoms within the interaction range. Therefore, the meshless AFEM is able to obtain the global stiffness matrix without element assembly and thus reduce the computational cost. This summation over all atoms within the interaction range is similar to element assembly used in AFEM (as well as in conventional FEM), but does not involve the "element" concept; the meshless AFEM is able to study the structural evolution without element re-generation.

Structural Evolution

Both external load and disordered disturbance (e.g., thermal fluctuation) about each atom's static equilibrium position lead to structural evolution. From the thermodynamics perspective, the disordered disturbance is given by Equation 16, where δ is the vector of disturbance and ranf() is a random number between 0 and 1. The molecular dy-

Equations

$$\mathbf{Ku} = \mathbf{P} \tag{10}$$

$$\mathbf{K} = \left.\frac{\partial^2 E_{tot}}{\partial \mathbf{x}\partial \mathbf{x}}\right|_{\mathbf{x}=\mathbf{x}^{(0)}} = \left.\frac{\partial^2 U_{tot}}{\partial \mathbf{x}\partial \mathbf{x}}\right|_{\mathbf{x}=\mathbf{x}^{(0)}} \tag{11}$$

$$\mathbf{P} = -\left.\frac{\partial E_{tot}}{\partial \mathbf{x}}\right|_{\mathbf{x}=\mathbf{x}^{(0)}} = \bar{\mathbf{F}} - \left.\frac{\partial U_{tot}}{\partial \mathbf{x}}\right|_{\mathbf{x}=\mathbf{x}^{(0)}} \tag{12}$$

$$\mathbf{K}^{element} = \begin{bmatrix} \left(\frac{\partial^2 U_{tot}}{\partial \mathbf{x}_1 \partial \mathbf{x}_1}\right)_{3\times 3} & \left(\frac{1}{2}\frac{\partial^2 U_{tot}}{\partial \mathbf{x}_1 \partial \mathbf{x}_i}\right)_{3\times 27} \\ \left(\frac{1}{2}\frac{\partial^2 U_{tot}}{\partial \mathbf{x}_i \partial \mathbf{x}_1}\right)_{27\times 3} & (0)_{27\times 27} \end{bmatrix} \tag{13}$$

$$\mathbf{P}^{element} = \begin{bmatrix} \left(\bar{\mathbf{F}}_1 - \frac{\partial U_{tot}}{\partial \mathbf{x}_1}\right)_{3\times 1} \\ (0)_{27\times 1} \end{bmatrix} \tag{14}$$

$$\begin{cases} K_{ij} = \dfrac{\partial^2 U_{tot}}{\partial \mathbf{x}_i \partial \mathbf{x}_j}, & \text{if j is inside of } R^i \\ K_{ij} = 0, & \text{if j is outside of } R^i \end{cases} \tag{15}$$

$$\Delta \mathbf{x} = (\text{ranf}(\,) - 0.5)\,\delta \tag{16}$$

$$\mathbf{x}_{trial} = \mathbf{x}_{old} + \Delta \mathbf{x} \tag{17}$$

$$\mathbf{x}_{new} = \mathbf{x}_{trial} + \mathbf{u} \tag{18}$$

namics simulations were conducted at room temperature to determine the disturbance vector δ. The atomic position $\mathbf{x}_{trial}$ at the beginning of each incremental step (not in equilibrium) is the accumulation of the equilibrium position $\mathbf{x}_{old}$ for the previous incremental step (depending on external load) and the disturbance $\Delta\mathbf{x}$, as in Equation 17.

Based upon this atomic position $\mathbf{x}_{trial}$, bond breaking is then examined by checking if the bond length is larger than the cutoff distance ($R^{(2)}$ for Brenner's potential). If the bond breaks, the neighbors of atoms involved will be re-formed based on the interaction range and the new stiffness matrix $\mathbf{K}_{trial}$ and non-equilibrium force vector $\mathbf{P}_{trial}$ are determined. By solving the governing equation $\mathbf{K}_{trial}\,\mathbf{u} = \mathbf{P}_{trial}$, the equilibrium position $\mathbf{x}_{new}$ is obtained by Equation 18.

Next the total atomistic energy U_{new} for the new configuration due to disordered disturbance $\Delta\mathbf{x}$ is calculated. If $U_{new} < U_{old}$ (total system energy for previous atomic position $\mathbf{x}_{old}$), the disordered disturbance-induced new configuration is more energetically favorable and will be considered as an acceptable configuration (i.e., $\mathbf{x}_{new}$ will be the input for the next incremental step). Otherwise, the disturbance is unacceptable and the equilibrium position $\mathbf{x}_{old}$ is still the input for the next incremental step. Figure 4 demonstrates the program flowchart for studying the structural evolution by introducing disordered disturbance.

RESULTS

Figure 5 compares the computational cost of meshless AFEM with the original AFEM by studying carbon nanotube bending. Simulations were conducted for four (5,5) armchair carbon nanotubes with 400, 800, 1,600, and 3,200 atoms without involving bonding breakage. The carbon nanotubes, which are initially straight with two ends fixed, are subject to the same lateral force of 50 eV/nm = 8.0 nN in the middle. Central processing unit (CPU) times and deformed configurations for the four cases are shown in Figure 5. The meshless AFEM uses less CPU time than that for AFEM (on a personal computer with 2.8 GHz CPU and 1 GB memory). The high efficiency of the meshless AFEM is mainly due to bypassing the element assembling efforts involved in AFEM. Moreover, both meshless AFEM and AFEM display an approximate linear dependence on the system size N. This is because the above four cases have well-defined atomic structures and interatomic potentials as well as localized loads (only at the center of the carbon nanotubes).

The bond breakage and fracture of carbon nanotubes was studied following the procedure given in Figure 4. Figure 6 shows the force-strain curve for a perfect (5,5) carbon nanotube (without initial defect) and an initially defective (5,5) carbon nanotube (with initial defect) subject to tension. The defective carbon nanotube has four broken bonds before the axial tensile load is imposed. The planar configuration of the perfect and defective carbon nanotubes are shown in the inset of Figure 6. In order to compare with experiments, force-strain curve is used instead of conventional force-displacement curve. The disordered disturbance leads to bond breakage when the tensile strain reaches ~23% for the perfect (5,5) carbon nanotube and ~12% for the defective (5,5) carbon nanotube. For both cases, upon bond breakage, the force has a sudden drop and the carbon nanotubes quickly fracture, which indicates that the fracture of the carbon nanotube is brittle. A similar phenomenon was also observed in M.F. Yu et al.'s[33] experiments that showed a sudden drop of force curve when the tensile strain reaches the failure value. The fracture procedure of the defective (5,5) carbon nanotube is shown in Figure 7. Since the disturbance is randomly imposed based on Equation 16, the next broken

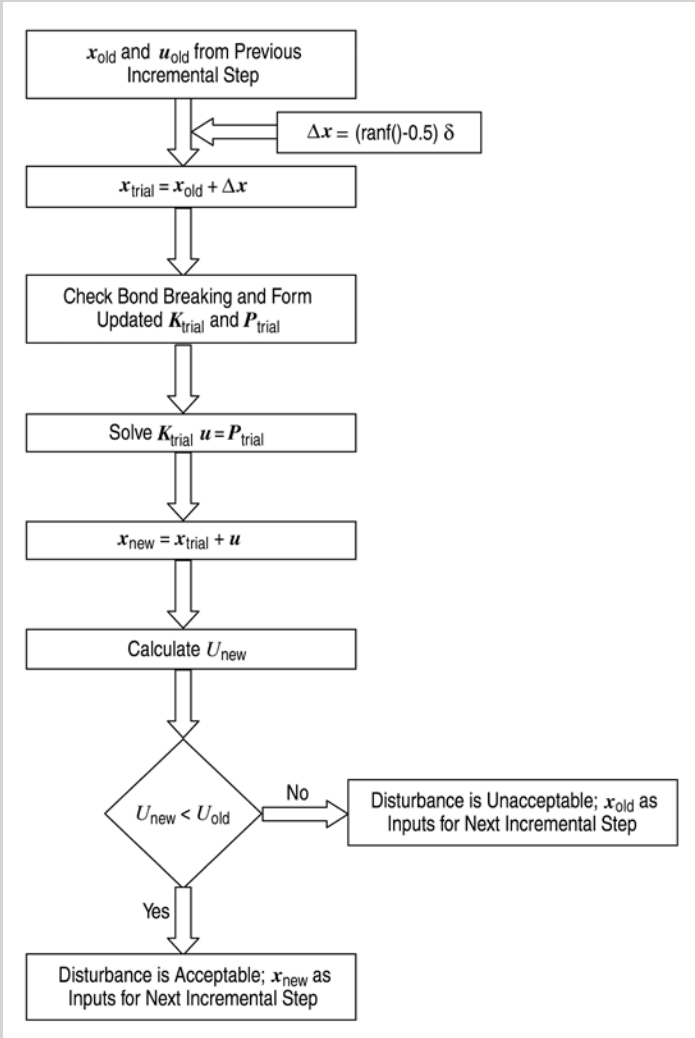

Figure 4. A flowchart on studying the structural evolution by introducing disordered disturbance using the meshless atomic-scale finite element method.

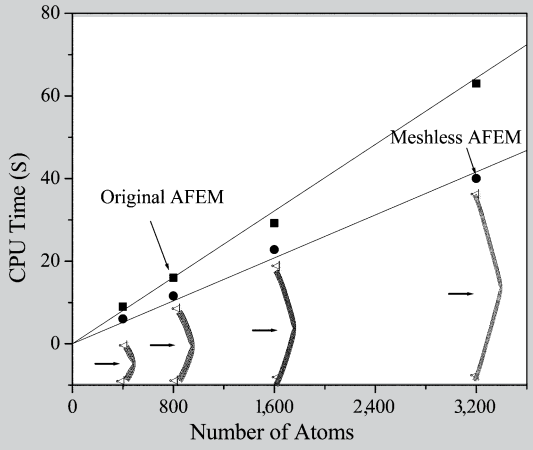

Figure 5. The CPU time of original and meshless atomic-scale finite element methods (AFEM) for four sets of (5,5) carbon nanotubes.

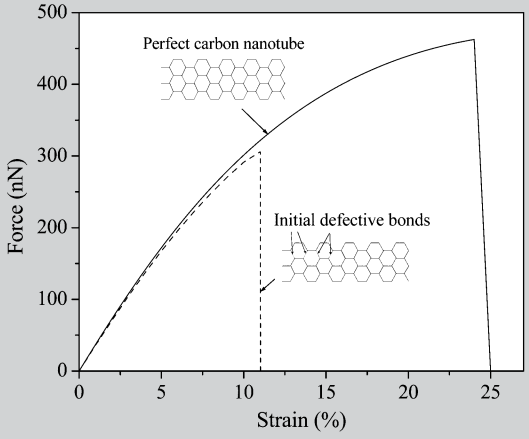

Figure 6. The force-strain relationship for a perfect (5,5) carbon nanotube and an initially defective (5,5) carbon nanotube.

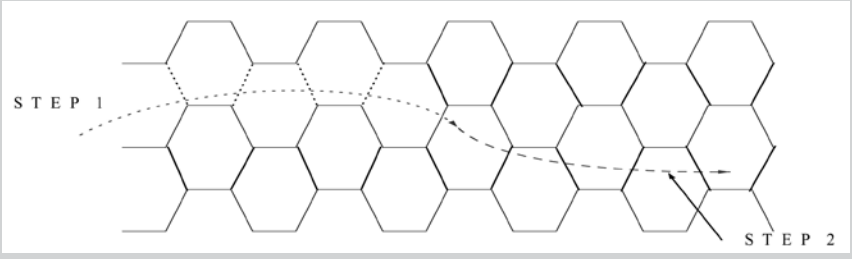

Figure 7. The fracture procedure of an initially defective (5,5) carbon nanotube.

bond is not pre-determined. Therefore, Figure 7 only shows one simulated fracture procedure among all possible ways. In the calculated fracture procedure, the fracture strain falls within a very narrow region of 12%.

CONCLUSION

By updating interaction range according to current positions of atoms, the proposed method can study the structural evolution of atomic structure. The fracture process and crack propagating of carbon nanotubes can be studied via the proposed method.

ACKNOWLEDGEMENT

Hanqing Jiang acknowledges the startup fund from Arizona State University. Yonggang Huang acknowledges the support from the Office of Naval Research (grant N00014-01-1-0205, Program Manager Dr. Y.D.S. Rajapakse), and NSFC.

References

1. J. Fish, *Journal of Nanoparticle Research,* 8 (5) (2006), pp. 577–594.
2. F.F. Abraham, *Proceedings of the National Academy of Sciences of the United States of America,* 99 (9) (2002), pp. 5777–5782.
3. F.F. Abraham et al., *Proceedings of the National Academy of Sciences of the United States of America,* 99 (9) (2002), pp. 5783–5787.
4. G.E. Moore, "Cramming More Components onto Integrated Circuits" (reprinted from *Electronics,* 19 April 1965, pp. 114–117), *Proceedings of the IEEE,* 86 (1) (1998), pp. 82–85.
5. D.W. Brenner et al., *Journal of Physics: Condensed Matter,* 14 (4) (2002), pp. 783–802.
6. D.W. Brenner, *Physical Review B,* 42 (15) (1990), pp. 9458–9471.
7. M. Arroyo and T. Belytschko, *Journal of the Mechanics and Physics of Solids,* 50 (9) (2002), pp. 1941–1977.
8. W.A. Curtin and R.E. Miller, *Modelling and Simulation in Materials Science and Engineering,* 11 (3) (2003), pp. R33–R68.
9. S. Curtarolo and G. Ceder, *Physical Review Letters,* 88 (25) (2002), p. 4.
10. W.N. E and Z.Y. Huang, *Physical Review Letters,* 8713 (13) (2001), p. 4.
11. S. Kohlhoff, P. Gumbsch, and H.F. Fischmeister, *Philosophical Magazine a-Physics of Condensed Matter Structure Defects and Mechanical Properties,* 64 (4) (1991), pp. 851–878.
12. H. Rafii-Tabar, L. Hua, and M. Cross, *Journal of Physics-Condensed Matter,* 10 (11) (1998), pp. 2375–2387.
13. R.E. Rudd and J.Q. Broughton, *Physica Status Solidi B-Basic Research,* 217 (1) (2000), pp. 251–291.
14. G.J. Wagner and W.K. Liu, *Journal of Computational Physics,* 190 (1) (2003), pp. 249–274.
15. W. Yang, H.L. Tan, and T.F. Guo, *Modelling and Simulation in Materials Science and Engineering,* 2 (3A) (1994), pp. 767–782.
16. D. Qian, G.J. Wagner, and W.K. Liu, *Computer Methods in Applied Mechanics and Engineering,* 193 (17-20) (2004), pp. 1603–1632.
17. W.K. Liu et al., *Computer Methods in Applied Mechanics and Engineering,* 195 (13-16) (2006), pp. 1407–1421.
18. S.Q. Tang, T.Y. Hou, and W.K. Liu, *Journal of Computational Physics,* 213 (1) (2006), pp. 57–85.
19. H.S. Park, E.G. Karpov, and W.K. Liu, *International Journal for Numerical Methods in Engineering,* 64 (2) (2005), pp. 237–259.
20. H. Kadowaki and W.K. Liu, *CMES–Computer Modeling in Engineering & Sciences,* 7 (3) (2005), pp. 269–282.
21. S.L. Zhang et al., *International Journal for Numerical Methods in Engineering,* 70 (8) (2007), pp. 913–933.
22. S.L. Zhang et al., *Physical Review B,* 71 (11) (2005), p. 12.
23. S.P. Xiao and T. Belytschko, *Computer Methods in Applied Mechanics and Engineering,* 193 (17-20) (2004), pp. 1645–1669.
24. V.B. Shenoy et al., *Journal of the Mechanics and Physics of Solids,* 47 (3) (1999), pp. 611–642.
25. R. Miller et al., *Engineering Fracture Mechanics,* 61 (3-4) (1998), pp. 427–444.
26. V.B. Shenoy et al., *Physical Review Letters,* 80 (4) (1998), pp. 742–745.
27. L.E. Shilkrot, W.A. Curtin, and R.E. Miller, *Journal of the Mechanics and Physics of Solids,* 50 (10) (2002), pp. 2085–2106.
28. E.B. Tadmor, R. Phillips, and M. Ortiz, *Langmuir,* 12 (19) (1996), pp. 4529–4534.
29. E.B. Tadmor, M. Ortiz, and R. Phillips, *Philosophical Magazine a-Physics of Condensed Matter Structure Defects and Mechanical Properties,* 73 (6) (1996), pp. 1529–1563.
30. M. Born and K. Huang, *Dynamical Theory of the Crystal Lattices* (Oxford: Oxford University Press, 1954).
31. B. Liu et al., *Physical Review B,* 72 (3) (2005), p. 8.
32. B. Liu et al., *Computer Methods in Applied Mechanics and Engineering,* 193 (17-20) (2004), pp. 1849–1864.
33. M.F. Yu et al., *Science,* 287 (5453) (2000), pp. 637–640.

Xue Feng and Bin Liu are with the Department of Engineering Mechanics, Tsinghua University, Beijing, 10084, P.R. China; Hanqing Jiang is with the Department of Mechanical and Aerospace Engineering, Arizona State University, Tempe, Arizona; Yonggang Huang is with the Department of Civil and Environmental Engineering and Department of Mechanical Engineering, Northwestern University, Evanston, Illinois; and Jiun-Shyan Chen is with the Department of Civil and Environmental Engineering, University of California, Los Angeles, California. Dr. Feng can be reached at fengxue@tsinghua.edu.cn and Dr. Jiang at hanqing.jiang@asu.edu.